



1 **Accelerated hydrological cycle over the Sanjiangyuan region induces**
2 **more streamflow extremes at different global warming levels**

3

4 Peng Ji^{1,2}, Xing Yuan³, Feng Ma³, Ming Pan⁴

5

6 ¹Key Laboratory of Regional Climate-Environment for Temperate East Asia, Institute
7 of Atmospheric Physics, Chinese Academy of Sciences, Beijing 100029, China

8 ²College of Earth and Planetary Sciences, University of Chinese Academy of Sciences,
9 Beijing 1000493, China

10 ³School of Hydrology and Water Resources, Nanjing University of Information
11 Science and Technology, Nanjing 210044, China

12 ⁴Department of Civil and Environmental Engineering, Princeton University, Princeton,
13 New Jersey, USA

14

15 *Correspondence to:* Xing Yuan (xyuan@nuist.edu.cn)



16 **Abstract.** Serving source water for the Yellow, Yangtze and Lancang-Mekong rivers,
17 the Sanjiangyuan region concerns ~700 million people over its downstream areas.
18 Recent research suggests that the Sanjiangyuan region will become wetter in a
19 warming future, but future changes in streamflow extremes remain unclear due to the
20 complex hydrological processes over high-land areas and limited knowledge of the
21 influences of land cover change and CO₂ physiological forcing. Based on high
22 resolution land surface modeling during 1979~2100 driven by the climate and
23 ecological projections from 11 newly released Coupled Model Intercomparison
24 Project Phase 6 (CMIP6) climate models, we show that different accelerating rates of
25 precipitation and evapotranspiration at 1.5 °C global warming level induce 55% more
26 dry extremes over Yellow river and 138% more wet extremes over Yangtze river
27 headwaters compared with the reference period (1985~2014). An additional 0.5 °C
28 warming leads to a further nonlinear and more significant increase for both dry
29 extremes over Yellow river (22%) and wet extremes over Yangtze river (64%). The
30 combined role of CO₂ physiological forcing and vegetation greening, which used to
31 be neglected in hydrological projections, is found to alleviate dry extremes at 1.5 and
32 2.0 °C warming levels but to intensify dry extremes at 3.0 °C warming level. Moreover,
33 vegetation greening contributes half of the differences between 1.5 and 3.0 °C
34 warming levels. This study emphasizes the importance of ecological processes in
35 determining future changes in streamflow extremes, and suggests a “dry gets drier,
36 wet gets wetter” condition over headwaters.

37 **Keywords** Terrestrial hydrological cycle, streamflow extremes, global warming levels,



38 CMIP6, Sanjiangyuan, land cover change



39 **1 Introduction**

40 Global temperature has been increasing at a rate of 1.7 °C/decade since 1970,
41 contrary to the cooling trend over the past 8000 years (Marcott et al., 2013). The
42 temperature measurements suggest that 2015-2019 is the warmest five years and
43 2010-2019 is also the warmest decade since 1850 (WMO, 2020). To mitigate the
44 impact of this unprecedented warming on the global environment and human society,
45 195 nations adopted the Paris Agreement which decides to “hold the increase in the
46 global average temperature to well below 2 °C above pre-industrial levels and pursuing
47 efforts to limit the temperature increase to 1.5 °C”.

48 The response of regional and global terrestrial hydrological processes, including
49 streamflow and its extremes, to different global warming levels has been investigated
50 by numerous studies in recent years (Chen et al., 2017; Döll et al., 2018; Marx et al.,
51 2018; Mohammed et al., 2017; Thober et al., 2018; Zhang et al., 2016). However, the
52 ecological factors (e.g., the CO₂ physiological forcing and land cover change), whose
53 importance in modulating the terrestrial hydrological responses is emphasized by
54 recent research, are often unaccounted for in studies regarding the changes in
55 hydrological extremes. For example, the suppression of stomatal conductance (thus
56 vegetation transpiration) by increased CO₂ concentration (known as the CO₂
57 physiological forcing), is found to alleviate the decreasing trend of streamflow in the
58 future at global scale (Wiltshire et al., 2013; Yang et al., 2019; Zhu et al., 2012).
59 While, the vegetation greening in a warming climate is found to have a significant
60 role on exacerbating hydrological drought, as it enhances transpiration and dries up



61 the land (Yuan et al., 2018b). Thus, it is necessary to assess their combined impacts on
62 the projection of streamflow extremes at different warming levels.

63 Hosting the headwaters of the Yellow river, the Yangtze river and the
64 Lancang-Mekong river, the Sanjiangyuan region is also known as the “Asian Water
65 Tower”. The alpine climate and fragile ecosystem make the Sanjiangyuan region
66 sensitive to the global warming (Kuang and Jiao, 2016; Liang et al., 2013; Yang et al.,
67 2013). Historical changes in climate and ecology (e.g. land cover) have significantly
68 altered the terrestrial hydrology and its extremes (Ji and Yuan, 2018; Yuan et al.,
69 2018a). For example, the Yellow river headwater region, which provides more than
70 one-third of the total streamflow in the Yellow river, experienced significant reduction
71 in mean and high flows during 1979-2005, increasing drought risk over its
72 downstream areas (Ji and Yuan, 2018). Recent research suggests that the
73 Sanjiangyuan region will become warmer and wetter in the future, and extreme
74 precipitation will also increase at the 1.5 °C global warming level and further intensify
75 with a 0.5 °C additional warming (Li et al., 2018; Zhao et al., 2019). However, how
76 the streamflow extremes would respond to the 1.5 °C warming, what an additional
77 0.5 °C or even greater warming would cause, and how much contributions do the
78 ecological factors (e.g., CO₂ physiological forcing and land cover change) have, are
79 still unknown. This makes it difficult to assess the climate and ecological impact on
80 this vital headwaters region.

81 In this study, we investigate the future changes in the streamflow extremes over
82 the Sanjiangyuan region from an integrated eco-hydrological perspective by taking



83 CO₂ physiological forcing and land cover change into consideration. The combined
84 impacts of the above two ecological factors at different global warming levels are also
85 quantified and compared with the impact of climate change. The results will help
86 understand the role of ecological factors in future terrestrial hydrological changes
87 over the headwater regions like the Sanjiangyuan, and provide guidance and support
88 for the stakeholders to make relevant decisions and plans.

89 **2 Data and methods**

90 **2.1 Observational Data**

91 Streamflow observations from the Tangnaihai (TNH) and the Zhimenda (ZMD)
92 hydrological stations (Figure 1a), which were provided by the local authorities, were
93 used to evaluate the streamflow simulations. Data periods are 1979-2011 and
94 1980-2008 for the Tangnaihai and Zhimenda stations individually. Monthly terrestrial
95 water storage change observation and its uncertainty during 2003-2014 was provided
96 by the Jet Propulsion Laboratory (JPL), which used the mass concentration blocks
97 (mascons) basis functions to fit the Gravity Recovery and Climate Experiment
98 (GRACE) satellite's inter-satellite ranging observations (Watkins et al., 2015). The
99 Model Tree Ensemble evapotranspiration (MTE_ET; Jung et al., 2009) and the Global
100 Land Evaporation Amsterdam Model evapotranspiration (GLEAM_ET) version 3.3a
101 (Martens et al., 2017) were also used to evaluate the model performance on ET
102 simulation.

103 **2.2 CMIP6 Data**

104 Here, 19 Coupled Model Intercomparison Project phase 6 (CMIP6, Eyring et al.,



105 2016) models which provide precipitation, near-surface temperature, specific
106 humidity, 10-m wind speed, surface downward shortwave and longwave radiations at
107 daily timescale were first selected for evaluation. Then, 11 of them were chosen for
108 the analysis as they can best reproduce the increasing precipitation over the
109 Sanjiangyuan region during 1979-2014 (Table 1). For the future projection
110 (2015-2100), we chose two Shared Socioeconomic Pathways (SSP) experiments:
111 SSP585 and SSP245. SSP585 combines the fossil-fueled development socioeconomic
112 pathway and 8.5W/m^2 forcing pathway (RCP8.5), while SSP245 combines the
113 moderate development socioeconomic pathway and 4.5 W/m^2 forcing pathway
114 (RCP4.5) (O'Neill et al., 2016). Land cover change is quantified by leaf area index
115 (LAI) as there is no significant transition between different vegetation types (not
116 shown) according to the Land-use Harmonization 2 (LUH2) dataset
117 (<https://esgf-node.llnl.gov/search/input4mips/>). For the CNRM-CM6-1, FGOALS-g3
118 and CESM2, the ensemble mean of LAI simulations from the other 8 CMIP6 models
119 was used because CNRM-CM6-1 and FGOALS-g3 do not provide dynamic LAI
120 while the CESM2 simulates an abnormally large LAI over the Sanjiangyuan region.
121 To avoid systematic bias in meteorological forcing, the trend-preserved bias
122 correction method suggested by ISI-MIP (Hempel et al., 2013), was applied to the
123 CMIP6 model simulations at monthly scale. The China Meteorological Forcing
124 Dataset (CMFD) is taken as meteorological observation (He et al., 2020). For each
125 month, temperature bias in CMIP6 simulations during 1979-2014 was directly
126 deducted. Future temperature simulations in SSP245 and SSP585 experiments were



127 also adjusted according to the historical bias. Other variables were corrected by using
128 a multiplicative factor, which was calculated by using observations to divide
129 simulation during 1979-2014. In addition, monthly leaf area index was also adjusted
130 to be consistent with satellite observation using the same method as temperature. All
131 variables were first interpolated to the 10km resolution over the Sanjiangyuan region
132 and the bias correction was performed for each CMIP6 model at each grid. After bias
133 correction, absolute changes of temperature and leaf area index, and relative changes
134 of other variables were preserved at monthly time scale (Hempel et al., 2013). Then,
135 the adjusted CMIP6 daily meteorological forcings were disaggregated into hourly
136 using the diurnal cycle ratios from the China Meteorological Forcing Dataset (CMFD;
137 He et al., 2020).

138 The historical CO₂ concentration used here is the same as the CMIP6 historical
139 experiment (Meinshausen et al., 2017), while future CO₂ concentration in SSP245 and
140 SSP585 scenarios came from simulations of a reduced-complexity carbon-cycle
141 model MAGICC7.0 (<http://greenhousegases.science.unimelb.edu.au/>).

142 **2.3 Experimental design**

143 The land surface model used in this study is the Conjunctive Surface-Subsurface
144 Process model version 2 (CSSPv2) (Yuan et al., 2018a). The CSSPv2 considers the
145 lateral transport of surface and subsurface water, incorporates the variable infiltration
146 capacity runoff scheme, and considers hydrological influences of soil organic matters.
147 Systematic evaluation has proved that CSSPv2 well simulates the energy and water
148 processes over the Sanjiangyuan region (Yuan et al., 2018a). Parameterization of the



149 stomatal conductance (g_s) in CSSPv2 is

$$150 \quad g_s = m \frac{A_n}{P_{CO_2} / P_{atm}} h_s + b \beta_t$$

151 where the m is a plant functional type dependent parameter, A_n is leaf net
152 photosynthesis ($\mu mol CO_2 m^{-2} s^{-1}$), P_{CO_2} is the CO_2 partial pressure at the leaf
153 surface (Pa), P_{atm} is the atmospheric pressure (Pa), h_s is the leaf surface
154 humidity, b is the minimum stomatal conductance ($\mu mol m^{-2} s^{-1}$), while β_t is the
155 soil water stress function. This parameterization is also used in the Community Land
156 Surface Model (CLM) and the Common Land Surface Model (CoLM). Generally, the
157 stomatal conductance decreases with the increasing of CO_2 concentration.

158 First, bias-corrected meteorological forcings from CMIP6 historical experiment
159 were used to drive the CSSPv2 model (CMIP6_His/CSSPv2). All simulations were
160 conducted for two cycles during 1979-2014 at half-hourly time step and 10 km spatial
161 resolution, with the first cycle serving as the spin-up.

162 Second, bias-corrected meteorological forcings in SSP245 and SSP585 were
163 used to drive CSSPv2 during 2015-2100 with dynamic LAI and CO_2 concentration
164 (CMIP6_SSP/CSSPv2). Initial conditions of CMIP6_SSP/CSSPv2 came from the last
165 year in CMIP6_His/CSSPv2.

166 Then, the second step was repeated twice by fixing the monthly LAI
167 (CMIP6_SSP/CSSPv2_FixLAI) and mean CO_2 concentration
168 (CMIP6_SSP/CSSPv2_FixCO2) at 2014 level. The difference between
169 CMIP6_SSP/CSSPv2 and CMIP6_SSP/CSSPv2_FixLAI is regarded as the net effect
170 of land cover change, and the difference between CMIP6_SSP/CSSPv2 and



171 CMIP6_SSP/CSSPv2_FixCO2 is regarded as the net effect of CO₂ physiological
172 forcing.

173 **2.4 Warming level determination**

174 A widely used time-sampling method was adopted to determine the periods of
175 different global warming levels (Chen et al., 2017; Döll et al., 2018; Marx et al., 2018;
176 Mohammed et al., 2017; Thober et al., 2018). According to the HadCRUT4 dataset
177 (Morice et al., 2012), the global mean surface temperature has increased by 0.66 °C
178 from the pre-industrial era (1850-1900) to the reference period defined as 1985-2014.
179 Then, starting from 2015, 30-years running mean global temperatures were compared
180 to those of the 1985-2014 period for each GCM simulation. And the
181 1.5 °C/2.0 °C/3.0 °C warming period is defined as the 30-years period when the
182 0.84 °C/1.34 °C/2.34 °C global warming, compared with the reference period
183 (1985-2014), is first reached. The median years of identified 30-year periods, referred
184 as “crossing years”, are shown in Table 2.

185 **2.5 Definition of dry and wet extremes**

186 In this research, the standardized streamflow index (SSI) was used to define dry
187 and wet extremes (Vicente-Serrano et al., 2012; Yuan et al., 2017). A gamma
188 distribution was first fitted using July-September (flood season) mean streamflow
189 during the reference period. Then the fitted distribution was used to calculate the
190 standardized deviation of the July-September mean streamflow (i.e. SSI) in each year
191 during both the reference and projection periods. Here, dry and wet extremes were
192 defined as where SSIs are smaller than -1.28 (a probability of 10%) and larger than



193 1.28 respectively.

194 **3 Results**

195 **3.1 Terrestrial hydrological changes at different warming levels**

196 As shown in Figures 1b-1e, the ensemble means of CMIP6 simulations (black
197 lines) can reproduce the historical increasing trends of temperature, precipitation and
198 LAI (pink lines) reasonably well. In 2015-2100, the SSP245 scenario (blue lines)
199 shows continued warming, wetting and greening trends, and the trends are larger in
200 the SSP585 scenario (red lines). The CO₂ concentration also keeps increasing during
201 2015-2100 and reaches to 600 ppm and 1150 ppm in 2100 for the SSP245 and
202 SSP585 scenarios respectively. Although the SSP585 scenario reaches the same
203 warming levels earlier than the SSP245 scenario (Table 2), there is no significant
204 difference between them in the meteorological variables during the same warming
205 period (not shown). Thus, we do not distinguish SSP245 and SSP585 scenarios at the
206 same warming level in the following analysis.

207 Figure 2 shows the evaluation of model simulation. Driven by observed
208 meteorological and ecological forcings, the CMFD/CSSPv2 simulates monthly
209 streamflow over the Yellow and Yangtze river headwaters quite well. Compared with
210 the observation at Tangnaihui (TNH) and Zhimenda (ZMD) stations, the Kling-Gupta
211 efficiencies of the CMFD/CSSPv2 simulated monthly streamflow are 0.94 and 0.91
212 respectively. The simulated monthly Terrestrial Water Storage Anomaly (TWSA)
213 during 2003-2014 in CMFD/CSSPv2 also agrees with the GRACE satellite
214 observation and captures the increasing trend. For the interannual variations of



215 evapotranspiration, CMFD/CSSPv2 is consistent with the ensemble mean of the
216 GLEAM_ET and MTE_ET products, and the correlation coefficient and root mean
217 squared error (RMSE) during 1982-2011 are 0.87 ($p < 0.01$) and 14 mm/year
218 respectively. This suggests the good performance of the CSSPv2 in simulating the
219 hydrological processes over the Sanjiangyuan region. Although meteorological and
220 ecological outputs from CMIP6 models have coarse resolutions (~100km), the land
221 surface simulation driven by bias corrected CMIP6 results (CMIP6_His/CSSPv2) also
222 captures the terrestrial hydrological variations reasonably well. The Kling-Gupta
223 efficiency of the ensemble mean streamflow simulation reaches up to 0.71~0.81, and
224 the ensemble mean monthly Terrestrial Water Storage Anomaly (TWSA) and annual
225 evapotranspiration generally agree with observations and other reference data
226 (Figures 2c-d).

227 Figure 3 shows relative changes of terrestrial hydrological variables over the
228 Sanjiangyuan region at different warming levels. The ensemble mean of the increase
229 in annual precipitation is 5% at 1.5 °C warming level, and additional 0.5 °C and 1.5 °C
230 warming will further increase the wetting trends to 7% and 13% respectively. Annual
231 evapotranspiration experiences significant increases at all warming levels, and the
232 ensemble mean increases are 4%, 7% and 13% at 1.5, 2.0 and 3.0 °C warming levels
233 respectively. The ratio of transpiration to evapotranspiration also increases
234 significantly, indicating that vegetation transpiration increases much larger than the
235 soil evaporation and canopy evaporation. Although annual total runoff has larger
236 relative changes than evapotranspiration (6%, 9% and 14% at 1.5, 2.0 and 3.0 °C



237 warming levels respectively), the uncertainty is large as only 75% of the models show
238 positive signals, which may be caused by large uncertainty in the changes during
239 summer and autumn seasons. The terrestrial water storage (TWS) which includes
240 foliage water, surface water, soil moisture and groundwater, shows slightly decreasing
241 trend at both annual and seasonal scales, however, changes little at the three warming
242 levels, suggesting that the increasing precipitation in the future becomes extra
243 evapotranspiration and runoff instead of recharging the local water storage. The
244 accelerated terrestrial hydrological cycle also exists at seasonal scale, as the seasonal
245 changes are consistent with the annual ones.

246 **3.2 Changes in streamflow extremes at different warming levels**

247 Although the intensified terrestrial hydrology induces more streamflow over the
248 headwater region of Yellow river during winter and spring months, streamflow does
249 not increase and even decreases during the flood season (July-September; Figure 4a).
250 Moreover, the frequency of streamflow dry extremes over the Yellow river is found to
251 increase by 55% at 1.5 °C warming level (Figure 4b), suggesting that abnormally low
252 streamflow will occur more frequently during the flood seasons in the future. The dry
253 extreme frequency will further increase to 77% and 125% at the 2.0 and 3.0 °C
254 warming levels and the results are more significant (Figure 4b). No significant
255 changes are found for the wet extremes at all warming levels over the Yellow River
256 headwater region.

257 Over the Yangtze river headwater region, streamflow increases in all months at
258 different warming levels (Figure 4c). The frequency of wet extremes increases



259 significantly by 138%, 202% and 232% at 1.5, 2.0 and 3.0 °C warming levels (Figure
260 4d), suggesting a higher risk of flooding. Moreover, the frequency of dry extremes
261 tends to decrease significantly by 35%, 44%, 34% at the three warming levels, but the
262 changes are much smaller than those of the wet extremes. Thus, we mainly focus on
263 the dry extremes over the Yellow river and the wet extremes over the Yangtze river in
264 the following analysis.

265 Different changes of streamflow extremes over the Yellow and Yangtze rivers
266 can be interpreted from different accelerating rates of precipitation and
267 evapotranspiration. Figure 5 shows probability density functions (PDFs) of
268 precipitation, evapotranspiration and their difference (P-ET, i.e. residual water for
269 runoff generation) during the flood season. Over the Yellow river, PDFs of
270 precipitation and evapotranspiration both shift to the right against the reference period.
271 However, the increasing trend of evapotranspiration is stronger than that of
272 precipitation, leading to a left shift of PDF for P-ET. Moreover, increased variations
273 of precipitation and evapotranspiration, as indicated by the increased spread of their
274 PDFs, also lead to a larger spread of PDFs of P-ET. The above two factors together
275 induce a heavier left tail in the PDF of P-ET for the warming future than the reference
276 period (Figure 5e). This indicates a higher probability of less water left for runoff
277 generation at different warming levels, given little changes in TWS (section 3.1).
278 Moreover, Figure 3e also shows little change to the right tails in the PDF of P-ET
279 (P-ET>130mm) at different warming levels, suggesting little change to the probability
280 of high residual water. This is consistent with the insignificant wet extreme change



281 over the Yellow river. Over the Yangtze river, however, intensified evapotranspiration
282 is much smaller than the increased precipitation, leading to a systematic rightward
283 shift of the PDF of P-ET (Figures 5b, 5d and 5f). Thus both the dry and wet extremes
284 show significant changes over the Yangtze river.

285 **3.3 Influences of land cover change and CO₂ physiological forcing**

286 Figures 6a-6b show the changes of streamflow extremes (compared with the
287 reference period) induced by climate and ecological factors. The CO₂ physiological
288 forcing tends to alleviate dry extremes (or increase wet extremes), while land cover
289 change plays a contrary role. Over the Yellow river, the combined impact of the two
290 ecological factors (sum of blue and cyan bars) reduces the increasing trend of dry
291 extremes caused by climate change (red bars) by 18~22% at 1.5 and 2.0 °C warming
292 levels, while intensifies the dry extremes by 9% at 3.0 °C warming level. This can be
293 interpreted from their contributions to the evapotranspiration, as the increased LAI
294 enhancement on ET is weaker than the suppression effect of CO₂ physiological
295 impact at 1.5 and 2.0 °C warming levels, while stronger at 3.0 °C warming level (not
296 shown). Over the Yangtze river, similarly, combined effect of land cover and CO₂
297 physiological forcing increases the wet extremes by 9% at 1.5 °C warming level while
298 decreases the wet extremes by 12% at 3.0 °C warming level. Thus, although climate
299 change plays the dominate role in inducing the extreme changes at different warming
300 levels, influences of CO₂ physiological forcing and land cover change are nontrivial.

301 In addition, Figures 6c and 6d show that the combined impact of CO₂
302 physiological forcing and land cover change also influences the differences between



303 different warming levels. Over the Yellow river, climate change increases dry
304 extremes by 26% from 1.5 to 2.0 °C warming level, and by 40% from 1.5 and 3.0 °C
305 warming level (red bars in Figure 6c). After considering the two ecological factors
306 (pink bars in Figure 6c), above two values change to 22% and 70% respectively, and
307 the difference between 1.5 and 3.0 °C warming levels becomes significant. For the wet
308 extreme over the Yangtze river (Figure 6d), the climate change induced difference
309 between 1.5 and 2.0 °C warming levels is decreased by 16% after accounting for the
310 two ecological factors. And this decrease reaches up to 49% for the difference
311 between 1.5 and 3.0 °C warming levels. We also compared the scenarios when CO₂
312 physiological forcing and land cover change are combined with climate change
313 individually (blue and cyan bars in Figures 6c-d), and the results show the land cover
314 change dominates their combined influences on the difference between different
315 warming levels.

316 **4 Conclusions and Discussion**

317 This study investigates changes of streamflow extremes over the Sanjiangyuan
318 region at different global warming levels through high-resolution land surface
319 modeling driven by CMIP6 climate simulations. The terrestrial hydrological cycle
320 under global warming of 1.5 °C is found to accelerate by 4~6% compared with the
321 reference period of 1985-2014. Although streamflow changes during the flood season
322 has a large uncertainty, the frequency of wet extremes over the Yangtze river will
323 increase significantly by 138% and that of dry extremes over the Yellow river will
324 increase by 55%. With an additional 0.5 °C warming, the frequency of dry and wet



325 extremes will increase further by 22~64%. If the global warming is not adequately
326 managed (e.g., to reach 3.0 °C), wet extremes over the Yangtze river and dry extremes
327 over the Yellow river will increase by 232% and 125%. Those nonlinear changes from
328 1.5 to 2.0 and 3.0 °C are also found for some fixed-threshold climate indices over the
329 Europe (Dosio and Fischer, 2018). It is necessary to cap the global warming at 2 °C or
330 even lower level, to reduce the risk of wet and dry extremes over the Yangtze and
331 Yellow rivers.

332 This study also shows the nontrivial contributions from land cover change and
333 CO₂ physiological forcing to the extreme streamflow changes especially at 2.0 and
334 3.0 °C warming levels. The CO₂ physiological forcing is found to increase streamflow
335 and reduce the dry extreme frequency by 14~24%, which is consistent with previous
336 research that CO₂ physiological forcing would increase available water and reduce
337 water stress at the end of this century (Wiltshire et al., 2013). However, our results
338 further show that the drying effect of increasing LAI on streamflow will exceed the
339 wetting effect of CO₂ physiological forcing at 3.0 °C warming level (during
340 2048~2075) over the Sanjiangyuan region, making a reversion in the combined
341 impacts of CO₂ physiological forcing and land cover. Thus it is vital to consider the
342 impact of land cover change in the projection of future water stress especially at high
343 warming scenarios.

344 Moreover, about 43~52% of the extreme streamflow changes between 1.5 and
345 3.0 °C warming levels are attributed to the increased LAI. Considering the LAI
346 projections from different CMIP6 models are induced by the climate change, it can be



347 inferred that the indirect influence of climate change (e.g., through land cover change)
348 has the same and even larger importance on the changes of streamflow extremes
349 between 1.5 and 3.0 °C or even higher warming levels, compared with the direct
350 influence (e.g., through precipitation and evapotranspiration). Thus, it is vital to
351 investigate hydrological and its extremes changes among different warming levels
352 from an eco-hydrological perspective instead of focusing on climate change alone.

353

354 **Acknowledgments** We thank the World Climate Research Programme's Working
355 Group on Couple modelling for providing CMIP6 data (<https://esgf-node.llnl.gov>).
356 This work was supported by National Key R&D Program of China
357 (2018YFA0606002) and National Natural Science Foundation of China (41875105,
358 91547103), and the Startup Foundation for Introducing Talent of NUIST.

359

360 **Competing interests**

361 The authors declare that they have no conflict of interest.

362



363 **References**

364 Chen, J., Gao, C., Zeng, X., Xiong, M., Wang, Y., Jing, C. Krysanova, V., Huang, J.,
365 Zhao, N., and Su, B.: Assessing changes of river discharge under global warming
366 of 1.5° C and 2° C in the upper reaches of the Yangtze River Basin: Approach
367 by using multiple-GCMs and hydrological models, *Quatern. Int.*, 453, 1 – 11,
368 <http://dx.doi.org/10.1016/j.quaint.2017.01.017>, 2017.

369 Döll, P., Trautmann, T., Gerten, D., Schmied, H. M., Ostberg, S., Saaed, F., and
370 Schleussner, C.: Risks for the global freshwater system at 1.5° C and 2° C
371 global warming. *Environ. Res. Lett.*, 13, 044038,
372 <https://doi.org/10.1088/1748-9326/aab792>, 2018.

373 Dosio, A., and Fischer, E. M.: Will half a degree make a difference? Robust
374 projections of indices of mean and extreme climate in Europe under 1.5° C, 2°
375 C, and 3° C global warming, *Geophys. Res. Lett.*, 45,
376 <https://doi.org/10.1002/2017GL076222>, 2018.

377 Eyring, V., Bony, S., Meehl, G. A., Senior, C. A., Stevens, B., Stouffer, R. J., and
378 Taylor, K. E.: Overview of the Coupled Model Intercomparison Project Phase 6
379 (CMIP6) experimental design and organization, *Geosci. Model Dev.*, 9, 1937 –
380 1958. <https://doi.org/10.5194/gmd-9-1937-2016>, 2016.

381 He, J., Yang, K., Tang, W., Lu, H., Qin, J., Chen, Y., and Li, X.: The first
382 high-resolution meteorological forcing dataset for land process studies over
383 China, *Sci. Data*, 7, 25. <https://doi.org/10.1038/s41597-020-0369-y>, 2020.

384



- 385 Hempel, S., Frieler, K., Warszawski, L., and Piontek, F.: A trend-preserving bias
386 correction-the ISI-MIP approach, *Earth Syst. Dyn.*, 4, 219-236.
387 <https://doi.org/10.5194/esd-4-219-2013>, 2013.
- 388 Ji, P., and Yuan, X.: High-resolution land surface modeling of hydrological changes
389 over the Sanjiangyuan region in the eastern Tibetan Plateau: 2. Impact of climate
390 and land cover change, *J. Adv. Model. Earth. Sy.*, 10, 2829 - 2843.
391 <https://doi.org/10.1029/2018MS001413>, 2018.
- 392 Jung, M., Reichstein, M., and Bondeau, A.: Towards global empirical upscaling of
393 FLUXNET eddy covariance observations: Validation of a model tree ensemble
394 approach using a biosphere model, *Biogeosciences*, 6, 2001–2013.
395 <https://doi.org/10.5194/bg-6-2001-2009>, 2009.
- 396 Kuang, X., and Jiao, J.: Review on climate change on the Tibetan Plateau during the
397 last half century, *J. Geophys. Res. Atmos.*, 121, 3979 - 4007.
398 <https://doi.org/10.1002/2015JD024728>, 2016.
- 399 Li, W., Jiang, Z., Zhang, X., Li, L. and Sun, Y.: Additional risk in extreme
400 precipitation in China from 1.5 ° C to 2.0 ° C global warming levels, *Sci.*
401 *Bull.*, 63, 228. <https://doi.org/10.1016/j.scib.2017.12.021>, 2018.
- 402 Liang, L., Li, L., Liu, C., and Cuo, L.: Climate change in the Tibetan Plateau Three
403 Rivers Source Region: 1960 - 2009, *Int. J. Climatol.*, 33, 2900-2916.
404 <https://doi.org/10.1002/joc.3642>, 2013.



- 405 Marcott, S. A., Shakun, J. D., Clark, P. U., and Mix, A. C.: A Reconstruction of
406 Regional and Global Temperature for the Past 11,300 Years, *Science*, 339, 1198
407 – 1201. <https://doi.org/10.1126/science.1228026>, 2013.
- 408 Martens, B., Miralles, D. G., Lievens, H., van der Schalie, R., de Jeu, R. A. M.,
409 Fernández-Prieto, D., Beck, H. E., Dorigo, W. A., and Verhoest, N. E. C.:
410 GLEAM v3: satellite-based land evaporation and root-zone soil moisture, *Geosci.*
411 *Model Dev.*, 10, 1903–1925. <https://doi.org/10.5194/gmd-10-1903-2017>, 2017.
- 412 Marx, A., Kumar, R., and Thober, S.: Climate change alters low flows in Europe
413 under global warming of 1.5, 2, and 3 ° C, *Hydrol. Earth. Syst. Sc.*, 22, 1017 –
414 1032. <https://doi.org/10.5194/hess-22-1017-2018>, 2018.
- 415 Meinshausen, M., Vogel, E., and Nauels, A., et al.: Historical greenhouse gas
416 concentrations for climate modelling (CMIP6), *Geosci. Model Dev.*, 10,
417 2057-2116. <https://doi.org/10.5194/gmd-10-2057-2017>, 2017.
- 418 Mohammed, K., Islam, A. S., Islam, G. M. T., Alfieri, L., Bala, S. K., and Khan, M. J.
419 U.: Extreme flows and water availability of the Brahmaputra River under 1.5 and
420 2 ° C global warming scenarios, *Climatic Change*, 145, 159-175.
421 <https://doi.org/10.1007/s10584-017-2073-2>, 2017.
- 422 Morice, C. P., Kennedy J. J., Rayner N. A., and Jones P. D.: Quantifying uncertainties
423 in global and regional temperature change using an ensemble of observational
424 estimates: The HadCRUT4 dataset, *J. Geophys. Res.*, 117, D08101.
425 <https://doi.org/10.1029/2011JD017187>, 2012.



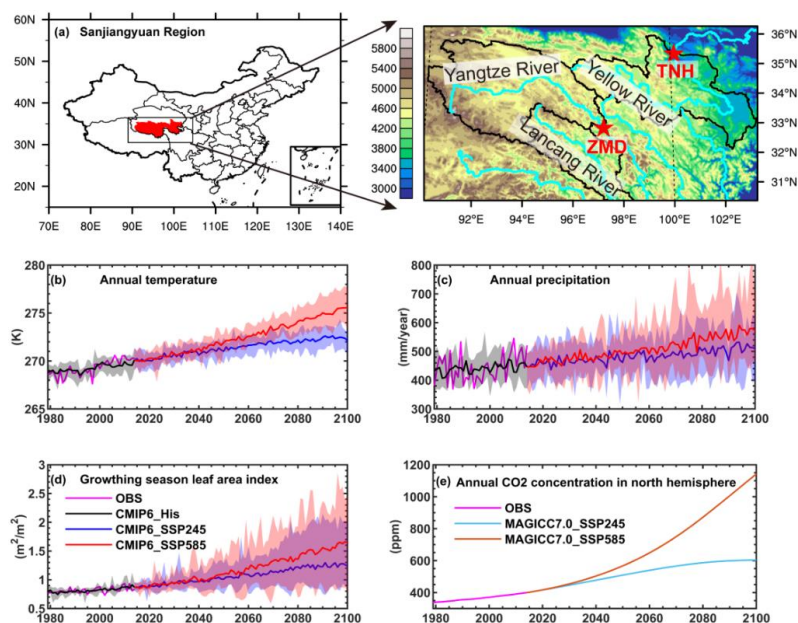
- 426 O'Neill, B. C., Tebaldi, C., Vuuren, D. P. V., Eyring, V., Friedlingstein, P., Hurtt, G.,
427 Knutti, R., Kriegler, E., Lamarque, J. F., Lowe, J., Meehl, G. A., Moss, R., Riahi,
428 K., and Sanderson, B. M.: The scenario model intercomparison project
429 (ScenarioMIP) for CMIP6, *Geosci. Model Dev.*, 9, 3461-3482.
430 <https://doi.org/10.5194/gmd-9-3461-2016>, 2016.
- 431 Thober, T., Kumar, R., and Waders, N.: Multi-model ensemble projections of
432 European river floods and high flows at 1.5, 2, and 3 degrees global warming,
433 *Environ. Res. Lett.*, 13, 014003. <https://doi.org/10.1088/1748-9326/aa9e35>,
434 2018.
- 435 Vicente-Serrano, S. M., Lopez-Moreno, J. I., Begueria, S., Lorenzo-Lacruz, J.,
436 Azorin-Molina, C., and Moran-Tejeda, E.: Accurate computation of a streamflow
437 drought index, *J. Hydrol. Eng.*, 17, 318 – 332.
438 [https://doi.org/10.1061/\(Asce\)He.1943-5584.0000433](https://doi.org/10.1061/(Asce)He.1943-5584.0000433), 2012.
- 439 Watkins, M. M., Wiese, D. N., Yuan, D. N., Boening, C., and Landerer, F. W.:
440 Improved methods for observing Earth's time variable mass distribution with
441 GRACE using spherical cap mascons, *J. Geophys. Res. Solid Earth*, 120,
442 2648-2671. <https://doi.org/10.1002/2014JB011547>, 2015.
- 443 Wiltshire, A., Gornall, J., Booth, B., Dennis, E., Falloon, P., Kay, G., McNeill, D.,
444 McSweeney, C. and Betts, R.: The importance of population, climate change and
445 CO2 plant physiological forcing in determining future global water stress, *Global*
446 *Environ. Change*, 23(5), 1083-1097.
447 <http://dx.doi.org/10.1016/j.gloenvcha.2013.06.005>, 2013.



- 448 WMO.: WMO Statement on the State of the Global Climate in 2019,
449 https://library.wmo.int/doc_num.php?explnum_id=10211, 2020.
- 450 Yang, K., Wu, H., Qin, J., Lin, C., Tang, W., and Chen, Y.: Recent climate changes
451 over the Tibetan plateau and their impacts on energy and water cycle: A review,
452 *Global Planet. Change*, 112, 79 – 91.
453 <https://doi.org/10.1016/j.gloplacha.2013.12.001>, 2013.
- 454 Yang, Y., Rodericj, M. L., Zhang, S., McVicar, T. R., and Donohue, R. J.: Hydrologic
455 implications of vegetation response to elevated CO₂ in climate projections, *Nat.*
456 *Clim. Change*, 9, 44-48. <https://doi.org/10.1038/s41558-018-0361-0>, 2019.
- 457 Yuan, X., Ji, P., Wang, L., Liang, X., Yang, K., Ye, A., Su, Z., and Wen, J.: High
458 resolution land surface modeling of hydrological changes over the Sanjiangyuan
459 region in the eastern Tibetan Plateau: 1. Model development and evaluation, *J.*
460 *Adv. Model. Earth. Sy.*, 10, 2806 – 2828. <https://doi.org/10.1029/2018MS001413>,
461 2018a.
- 462 Yuan, X., Jiao, Y., Yang, D., and Lei, H.: Reconciling the attribution of changes in
463 streamflow extremes from a hydroclimate perspective, *Water Resour. Res.*, 54,
464 3886 – 3895. <https://doi.org/10.1029/2018WR022714>, 2018b.
- 465 Yuan, X., Zhang, M., Wang, L., and Zhou, T.: Understanding and seasonal forecasting
466 of hydrological drought in the Anthropocene, *Hydrol. Earth. Syst. Sc.*, 21, 5477
467 – 5492. <https://doi.org/10.5194/hess-21-5477-2017>, 2017.



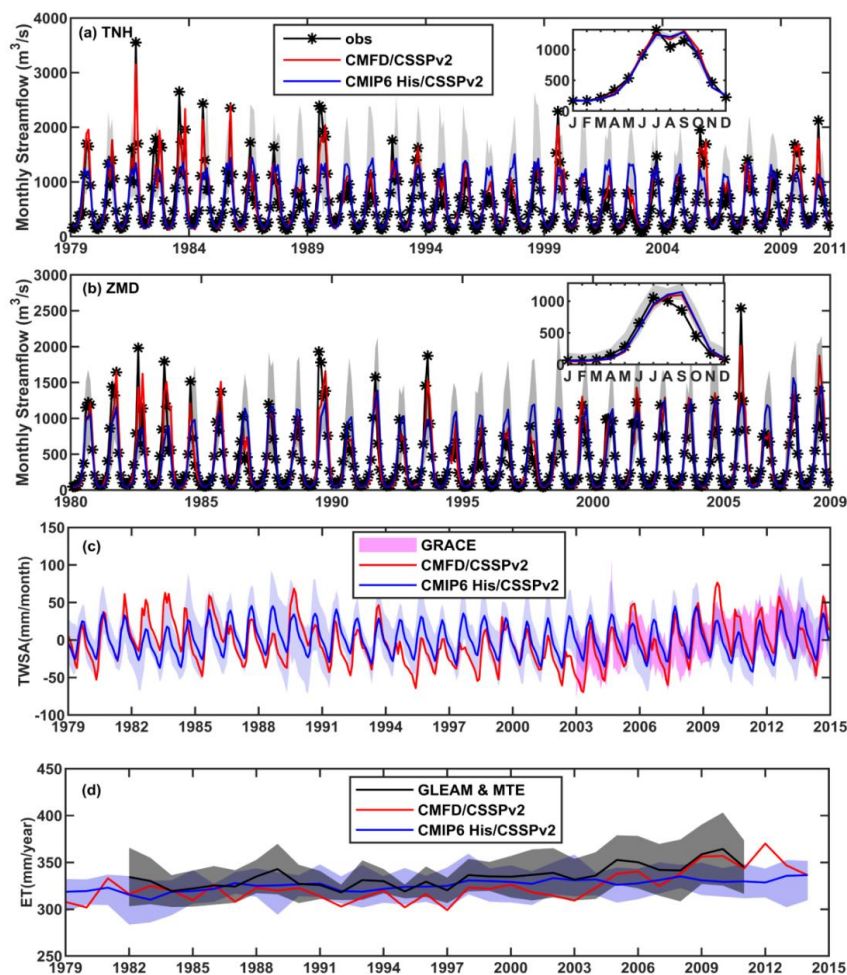
- 468 Zhang Y., You Q., Chen C., and Ge J.: Impacts of climate change on streamflows
469 under RCP scenarios: A case study in Xin River Basin, China, Atmos. Res.,
470 178-179, 521-534. <http://dx.doi.org/10.1016/j.atmosres.2016.04.018>, 2016.
- 471 Zhao Q., Ding Y., Wang J., Gao H., Zhang S., Zhao C. Xu J. Han H., and Shangguan
472 D.: Projecting climate change impacts on hydrological processes on the Tibetan
473 Plateau with model calibration against the glacier inventory data and observed
474 streamflow, J. Hydrol., 573, 60-81. <https://doi.org/10.1016/j.jhydrol.2019.03.043>,
475 2019.
- 476 Zhu Q., Jiang H., Peng C., Liu J., Fang X., Wei X., Liu S., and Zhou G: Effects of
477 future climate change, CO2 enrichment, and vegetation structure variation on
478 hydrological processes in China, Global Planet. Change, 80-81, 123-135.
479 <https://doi.org/10.1016/j.gloplacha.2011.10.010>, 2012.
- 480



481

482 **Figure 1.** (a) The locations of the Sanjiangyuan region and streamflow gauges. (b)-(e)
483 are the time series of annual temperature, precipitation, growing season leaf area
484 index and CO₂ concentration averaged over the Sanjiangyuan region during
485 1979-2100. Red pentagrams in (a) are two streamflow stations named Tangnaihai
486 (TNH) and Zhimenda (ZMD). Black, blue and red lines in (b-d) are ensemble means
487 of CMIP6 model simulations from the historical, SSP245 and SSP585 experiments.
488 Shadings are ranges of individual ensemble members. Cyan and brown lines in (e) are
489 future CO₂ concentration under SSP245 and SSP585 scenarios simulated by
490 MAGICC7.0 model.

491



492

493 **Figure 2.** Evaluation of model simulations. (a-b) Observed and simulated monthly
494 streamflow at the Tangnaihai (TNH) and Zhimenda (ZMD) hydrological stations, with
495 the climatology shown in the upper-right corner. (c-d) Evaluation of the simulated
496 monthly terrestrial water storage anomaly (TWSA) and annual evapotranspiration (ET)
497 averaged over the Sanjiangyuan region. Red lines are CSSPv2 simulation forced by
498 observed meteorological forcing. Blue lines represent ensemble means of 11
499 CMIP6_His/CSSPv2 simulations, while gray shadings in (a-b) and blue shadings in
500 (c-d) are ranges of individual ensemble members. Pink shading in (c) is GRACE

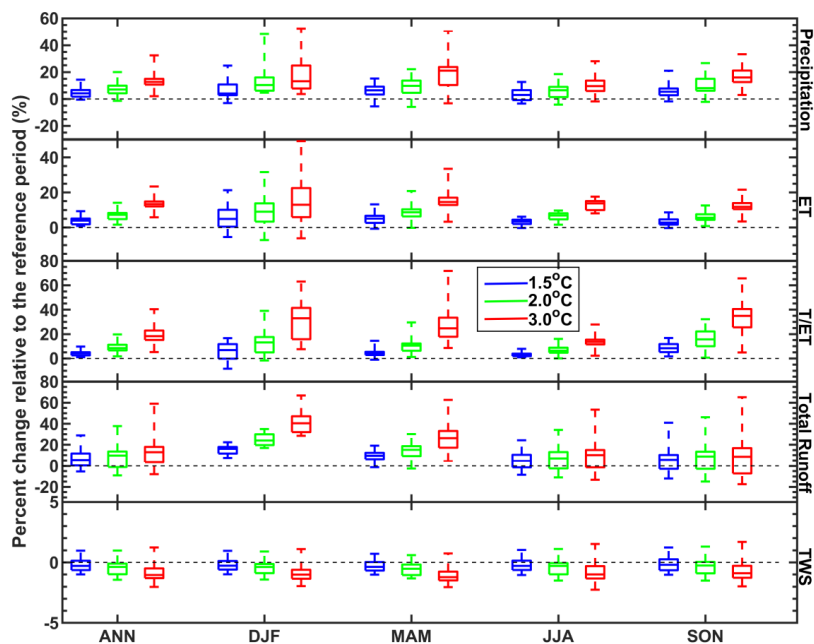


501 satellite observations. Black line and black shading in (d) are ensemble mean and

502 ranges of GLEAM_ET and MTE_ET datasets.

503

504

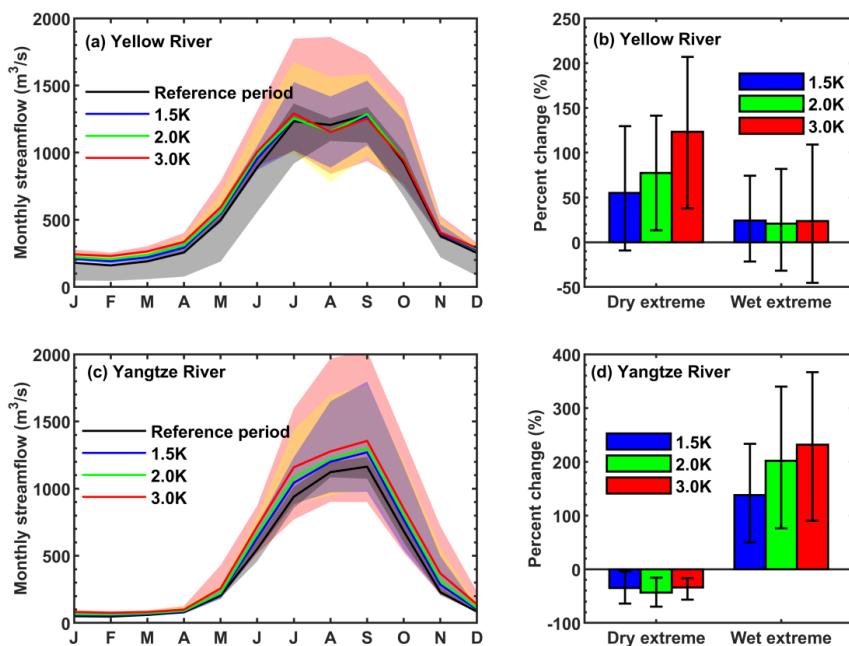


505

506 **Figure 3.** Box plots of relative changes of regional mean precipitation,
507 evapotranspiration (ET), ratio of transpiration to evapotranspiration (T/ET), total
508 runoff and terrestrial water storage (TWS) at different global warming levels.
509 Reference period is 1985-2014, and annual (ANN) and seasonal (winter: DJF, spring:
510 MAM, summer: JJA and autumn: SON) results are all shown. Boxes show 25th to
511 75th ranges among 22 CMIP6_SSP/CSSPv2 simulations, while lines in the boxes are
512 median values.



513

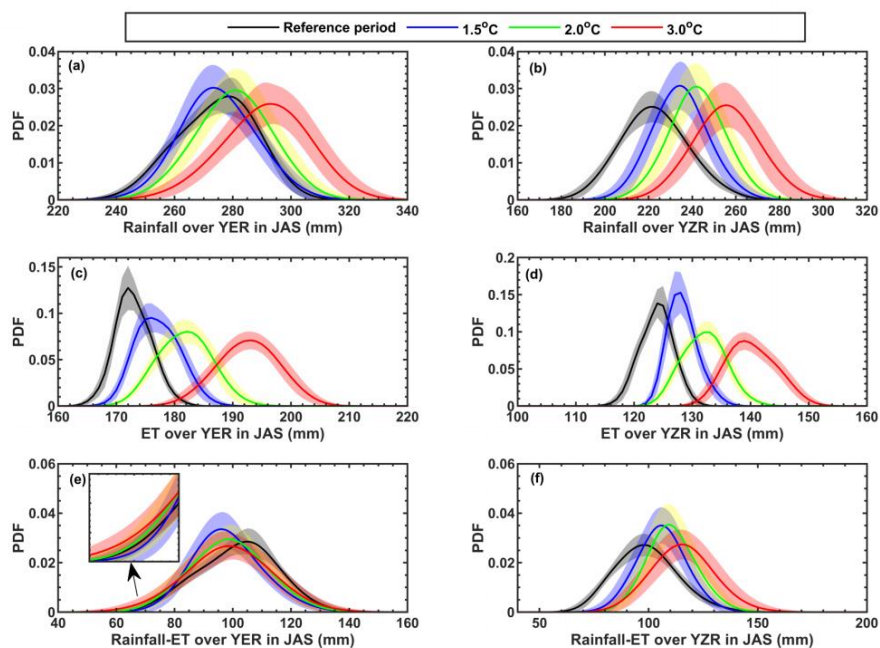


514

515 **Figure 4.** Changes of streamflow and its extremes at the outlets of the headwater
516 regions of the Yellow river and the Yangtze river, i.e., Tangnaihai gauge and
517 Zhimenda gauge. (a) Simulated monthly streamflow climatology over the Yellow
518 river during the reference period (1985-2014) and the periods with different global
519 warming levels. Solid lines represent ensemble means, while shadings are ranges of
520 individual ensemble members. (b) Percent changes in frequency of dry and wet
521 extremes in July-September at different warming levels. Colored bars are ensemble
522 means, while error bars are 5~95% uncertainty ranges estimated by using
523 bootstrapping for 10,000 times. (c) and (d) are the same as (a) and (b), but for the
524 Yangtze river.



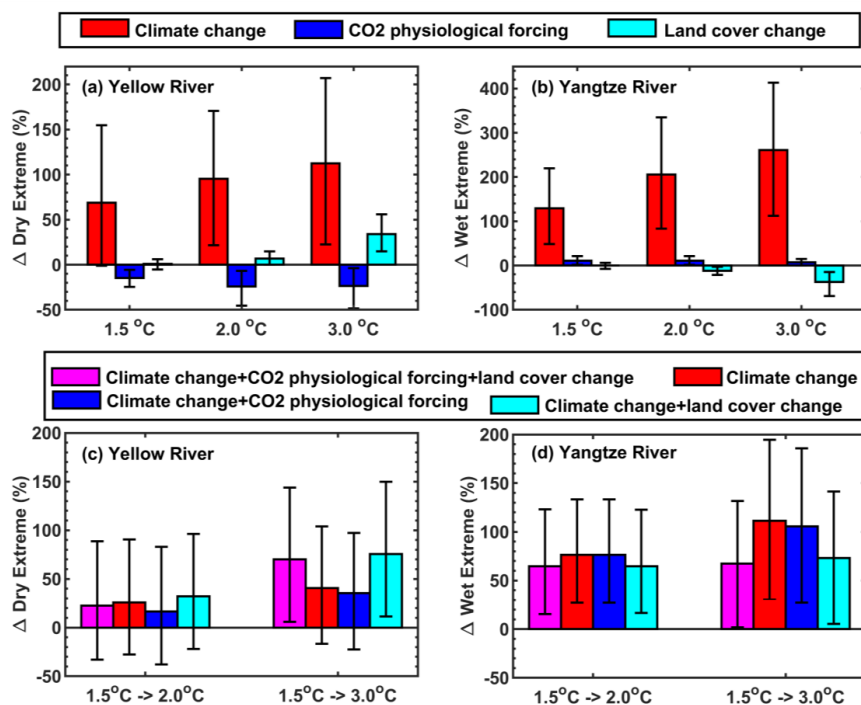
525



526

527 **Figure 5.** Probability density functions (PDFs) of regional mean rainfall,
528 evapotranspiration (ET) and their difference over the headwater regions of Yellow
529 river (YER) and Yangtze river (YZR) during flooding seasons (July-September) for
530 the reference period (1985-2014) and the periods with 1.5, 2.0 and 3.0 °C global
531 warming levels. Shadings are 5~95% uncertainty ranges.

532



533

534 **Figure 6.** (a-b) Influences of climate change, CO₂ physiological forcing and land
 535 cover change on relative changes in frequency of the dry and wet extremes in
 536 July-September at different global warming levels for the headwater regions of
 537 Yellow river and Yangtze river. (c-d) Changes of dry and wet extremes under
 538 additional warming of 0.5 °C and 1.5 °C with the consideration of different factors. All
 539 the changes are relative to the reference period (1985-2014). Ensemble means are
 540 shown by colored bars while the 5~95% uncertainty ranges estimated by using
 541 bootstrapping for 10,000 times are represented by error bars.

542



543 **Table 1.** CMIP6 simulations used in this study. His means historical simulations
 544 during 1979-2014 with both anthropogenic and natural forcings, SSP245 and SSP585
 545 represent two Shared Socioeconomic Pathways during 2015-2100. Note the
 546 CNRM-CM6-1 and CNRM-ESM2-1 do not provide r1i1p1f1 realization, so r1i1p1f2
 547 was used instead.

No.	Models	Experiments	Realization	Horizontal Resolution (Longitude × Latitude Grid Points)
1	ACCESS-ESM1-5	His/SSP245/SSP585	r1i1p1f1	192×145
2	BCC-CSM2-MR	His/SSP245/SSP585	r1i1p1f1	320×160
3	CESM2	His/SSP245/SSP585	r1i1p1f1	288×192
4	CNRM-CM6-1	His/SSP245/SSP585	r1i1p1f2	256×128
5	CNRM-ESM2-1	His/SSP245/SSP585	r1i1p1f2	256×128
6	EC-Earth3-Veg	His/SSP245/SSP585	r1i1p1f1	512×256
7	FGOALS-g3	His/SSP245/SSP585	r1i1p1f1	180×80
8	GFDL-CM4	His/SSP245/SSP585	r1i1p1f1	288×180
9	INM-CM5-0	His/SSP245/SSP585	r1i1p1f1	180×120
10	MPI-ESM1-2-HR	His/SSP245/SSP585	r1i1p1f1	384×192
11	MRI-ESM2-0	His/SSP245/SSP585	r1i1p1f1	320×160

548



549 **Table 2.** Determination of “crossing years” for the periods reaching 1.5, 2 and 3 °C
 550 warming levels for different GCM and SSP combinations.

Models	1.5 °C warming level		2.0 °C warming level		3.0 °C warming level	
	SSP245	SSP585	SSP245	SSP585	SSP245	SSP585
ACCESS-ESM1-5	2024	2023	2037	2034	2070	2052
BCC-CSM2-MR	2026	2023	2043	2034	Not found	2054
CESM2	2024	2022	2037	2032	2069	2048
CNRM-CM6-1	2032	2028	2047	2039	2075	2055
CNRM-ESM2-1	2030	2026	2049	2039	2075	2058
EC-Earth3-Veg	2028	2023	2044	2035	2072	2053
FGOALS-g3	2033	2032	2063	2046	Not found	2069
GFDL-CM4	2025	2024	2038	2036	2073	2053
INM-CM5-0	2031	2027	2059	2038	Not found	2063
MPI-ESM1-2-HR	2032	2030	2055	2044	Not found	2066
MRI-ESM2-0	2024	2021	2038	2030	2074	2051

551